Li2RuO3 as an Additive for High-Energy Lithium-Ion Capacitors

ARTICLE *in* THE JOURNAL OF PHYSICAL CHEMISTRY C · JANUARY 2013

Impact Factor: 4.77

1 AUTHOR:

Jung Ho Kim

University of Wollongong

183 PUBLICATIONS **1,949** CITATIONS

SEE PROFILE

THE JOURNAL OF PHYSICAL CHEMISTRY C

Article

pubs.acs.org/JPCC

Li_2RuO_3 as an Additive for High-Energy Lithium-Ion Capacitors

Min-Sik Park,[†] Young-Geun Lim,[†] Jung-Woo Park,[†] Jeom-Soo Kim,*[,†] Jong-Won Lee,[‡] Jung Ho Kim,[§] Shi Xue Dou,[§] and Young-Jun Kim*[,†]

[†]Advanced Batteries Research Center, Korea Electronics Technology Institute, 68 Yatap-dong, Bundang-gu, Seongnam 463-816, Republic of Korea

[‡]New and Renewable Energy Research Division, Korea Institute of Energy Research, 152 Gajeong-ro, Yuseong-gu, Daejeon 305-343, Republic of Korea

[§]Institute for Superconducting and Electronic Materials, University of Wollongong, North Wollongong, NSW2500, Australia

Supporting Information

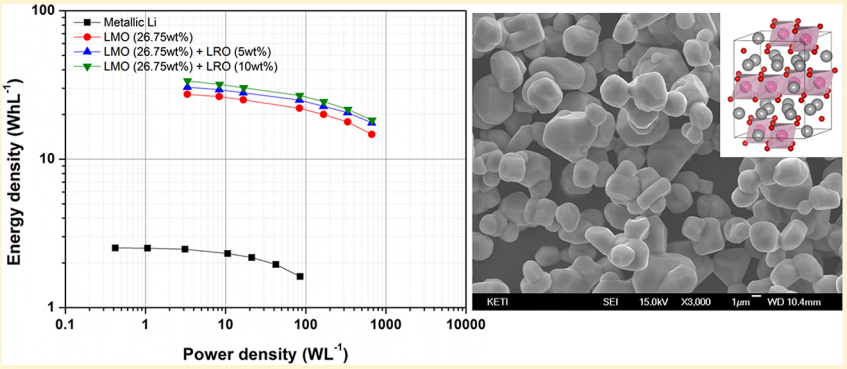

ABSTRACT: A high-energy lithium ion capacitor that has Li_2MoO_3 as an alternative lithium source instead of metallic lithium has been proposed. For further improvement, we suggest Li_2RuO_3 as a new additive to improve the energy density in the positive electrode. The choice of Li_2RuO_3 is made based on its highly reversible characteristics for Li^+ insertion and extraction and its structural stability in the operating voltage window of advanced lithium ion capacitors. The electrochemical and structural properties of Li_2RuO_3 have been thoroughly investigated to demonstrate its potential use in lithium ion capacitors. The high reversibility of Li_2RuO_3 and the metallic feature of $Li_{2-x}RuO_3$ may be responsible for improvements in the volumetric energy density and safety. This versatile approach may yield higher energy density without significant power loss in lithium ion capacitors.

INTRODUCTION

The lithium ion capacitor (LIC) has been proposed as an advanced energy-storage system combining the strengths of the lithium ion battery (LIB) with those of the electrochemical double-layer capacitor (EDLC). The LIC has an asymmetric cell configuration, consisting of an activated carbon positive electrode (PE) and Li^+ intercalating carbon material in the negative electrode (NE). The hybrid construction of the LIC makes it possible to achieve compatibility between high energy density (Wh/kg) and high power (W/L), so the LIC is suitable for applications that involve load balancing of renewable power generation and instantaneous voltage-drop compensation.[1,2] In principle, the high energy of the LIC results from the anodic reactions in the NE, which are mainly associated with Li^+ insertion and extraction at a low reaction potential (close to 0 V vs Li/Li^+) rather than with absorption and desorption of anions. Therefore, the LIC can exhibit extended high operating voltage of up to 4.2 V, which is much higher than that of the EDLC (3.0 V). Furthermore, the LIC features a higher power density than the LIB because the electrochemical reactions in the PE are mainly based on the absorption and desorption of anions. These attractive characteristics have fascinated many researchers who are interested in the development of advanced energy storage applications.[3−5]

Despite these considerable advantages, there are still challenges in the use of Li^+ intercalating materials in the NE. To achieve reversible Li^+ insertion and extraction in the NE, Li^+ predoping of the NE is compulsory prior to charging, as predoping is essential to controlling its electrochemical performance. The LIC commonly uses auxiliary metallic lithium for Li^+ predoping, causing significant safety concerns. Significant progress has been made in the Li^+ predoping process by introducing a transition-metal oxide, Li_2MoO_3, as the Li^+ source into the PE, as done in our previous work.[6] Li_2MoO_3, which has a high irreversibility of Li^+ intercalation (>70%), could successfully supply Li^+ into the carbon NE on

Received: January 18, 2013
Revised: May 8, 2013
Published: May 20, 2013

   dx.doi.org/10.1021/jp4005828 | J. Phys. Chem. C 2013, 117, 11471−11478

demand, where Li^+ can fully participate in the anodic reaction.[7−10] The Li^+ predoping process with Li_2MoO_3 improves the volumetric energy density and ensures safety by eliminating metallic lithium in the proposed system. The LIC energy density that can be achieved by applying an alternative Li^+ source, however, is still inadequate to meet performance requirements in the case of practical applications. Thus, we have focused on further increase in the energy density of the LIC.

In pursuit of energy improvement of the LIC, we intended to incorporate a potential additive into the PE within the current design of the LIC; Li_2MoO_3 was employed as the Li source. Although various transition-metal oxides and functional polymers have been considered as promising additives for providing pseudocapacitance in hybrid capacitors, careful consideration is required to make the right selection.[11−14] Therefore, we have rigorously applied our selection criteria: (i) The additive should have high capacity, reversibility, and structural stability in the operating voltage region of the LIC (1.5−4.2 V). (ii) The additive should contribute to providing additional electrochemical energy without sacrificing the electronic conductivity of the PE.[15−17]

Herein, we present Li_2RuO_3 as a promising additive to improve the energy density of the LIC. Li_2RuO_3 is one of many highly stable Li^+ intercalating compounds. Because of the significant metal−metal bonding between the Ru atoms, it facilitates good electronic and ionic conductivity. In addition, it can deliver high capacity with excellent reversibility, even at high current density, which could contribute to enhancement of the energy density of the LIC. Although Li_2RuO_3 has been considered as a potential cathode material with high capacity for use in the LIB, its feasibility in capacitor applications has not yet been demonstrated.[18−20] Our major concern is to investigate thoroughly the electrochemical and structural properties of Li_2RuO_3 as a potential additive for improving the energy density of LICs. In our proposed system, the role of Li_2RuO_3 is to promote the redox reactions of $Ru^{4+}/Ru^{5+}/Ru^{6+}$ in Li_2RuO_3 during cycling. Li_2RuO_3 would independently act as an active material and contribute additional energy to the LIC. This is unlike Li_2MoO_3, which provides Li^+ to the NE for prelithiation. The positive and negative effects of the addition of Li_2RuO_3 on the electrochemical properties of LICs will be discussed. Furthermore, the rational design of the PE to develop high-energy and high-power LICs will be emphasized.

EXPERIMENTAL SECTION

Materials Preparation. Li_2MoO_3 was synthesized by carbothermal reduction of Li_2MoO_4 with 7 wt % Super-P (TIMCAL), as described in our previous work.[6] Single-phase Li_2RuO_3 was prepared by a conventional solid-state reaction. Stoichiometric amounts (molar ratio of 1: 1) of RuO_2 nanopowder (Aldrich, 99.5%) and Li_2CO_3 (Aldrich, 99.9%) were thoroughly mixed and calcined at 900 °C for 12 h in air. Li_2CO_3 (3.5 mol %) was in excess to prevent undesirable lithium deficiency that may arise in the high-temperature process. The final product was carefully ground and used as an additive for LICs.

Structural Analyses. Powder X-ray diffraction (XRD) patterns and in situ XRD patterns were collected using an X-ray diffractometer (Empyrean, PAN analytical) equipped with a 3D pixel semiconductor detector using Cu−Kα radiation (λ = 1.54056 Å). The morphology and microstructure of Li_2RuO_3 were observed by field-emission scanning electron microscopy (FESEM, JEOL JSM-7000F) and high-resolution transmission electron microscopy (HRTEM, JEOL JEM3010). The particle size distribution was measured using a particle size analyzer (Microtrac S3500). The surface chemistry of $Li_{2-x}RuO_3$ was characterized by X-ray photoelectron spectroscopy (XPS, Thermo Scientific Sigma Probe).

Electrochemical Measurements. PEs were prepared by coating an Al mesh with a slurry containing the active materials (activated carbon + Li_2MoO_3 + Li_2RuO_3, 92 wt %) and binder (polyvinylidene fluoride (PVDF), 8 wt %) dissolved in *N*-methyl-2-pyrolidinone (NMP). The activated carbon and Li_2MoO_3 contents were fixed at 64.4 and 25.6 wt %, respectively, which correspond to 60% of anodic capacity. The amounts of Li_2RuO_3 in the PEs were 0, 5, and 10 wt %. Corresponding NEs were prepared by the same coating method using a Cu mesh instead of the Al mesh, using an active material (hard carbon, 80 wt %), a conducting agent (Super-P, 10 wt %), and a binder (PVDF, 10 wt %). After drying at 120 °C for 12 h under vacuum, the PE and NE were pressed and punched into discs with diameters of ø12 and ø14 mm, respectively. CR2032 coin-type half cells and full cells were carefully assembled with a porous polyethylene separator (ø19 mm) and electrolyte (100 μL). The electrolyte was prepared by dissolving 1.3 M $LiPF_6$ in a mixture of ethylene carbonate and dimethyl carbonate (3:7 v/v, Panax E-tec). Cyclic voltammetry (CV) measurements were carried out using a potentiostat/galvanostat (EC-Lab, Bio Logic). For Li^+ predoping, the potential was scanned linearly from open-circuit voltage (OCV) to 4.7 V (vs Li/Li^+) at a scan rate of 0.05 mV/s, and the potential scan direction was reversed to 2.5 V. Thereafter, more potential cycles were performed in the voltage range of 2.5 to 4.1 V at various scan rates. The ac-impedance measurements were performed using a Solartron 1255 frequency analyzer combined with Solartron 1287 ECI. The ac-impedance spectra were obtained by applying an ac-amplitude of 5 mV peak-to-peak over the frequency range of 10 mHz to 1 MHz. All electrochemical data were obtained at room temperature within an error range of 5%.

RESULTS AND DISCUSSION

Li_2RuO_3 was successfully synthesized through a conventional solid-state reaction by heating Li_2CO_3 and RuO_2 precursors. Figure 1a shows the XRD pattern of Li_2RuO_3. All reflections are well-matched with the typical pattern of Li_2RuO_3, which has a monoclinic symmetry (JCPDS 85-2000). There is no visible evidence of the formation of any impurity or secondary phase. From a detailed refinement, we found that Li_2RuO_3 is isostructural with Li_2MnO_3 (space group: *C2/c*). The calculated unit cell parameters of Li_2RuO_3 were as follows: a = 4.9327(4), b = 8.7759(0), and c = 9.8785(6) Å; these agree with the values reported in the literature.[21] Li_2RuO_3 has an identical cubic close-packed oxygen lattice, in which only Li^+ and a combination of $1/3Li^+$ and $2/3Ru^{4+}$ alternatively occupy octahedral sites. Therefore, it is expected that >1 mol of Li^+ could be electrochemically extracted from the given structures. The highly reversible characteristics of Li_2RuO_3 mainly originate from its symmetry, which is generally dependent on the ionic radius and the nature of the transition-metal bonding in the structure. Ru^{4+}, which has an ionic radius of 0.62 Å in the octahedral coordination, tends to form a monoclinic symmetry, which governs the redox reactions of $Ru^{4+}/Ru^{5+}/Ru^{6+}$ in the topotactic extraction and insertion of Li^+.[22] Further inspection of the morphology and microstructure of Li_2RuO_3 was

dx.doi.org/10.1021/jp4005828 | J. Phys. Chem. C 2013, 117, 11471−11478

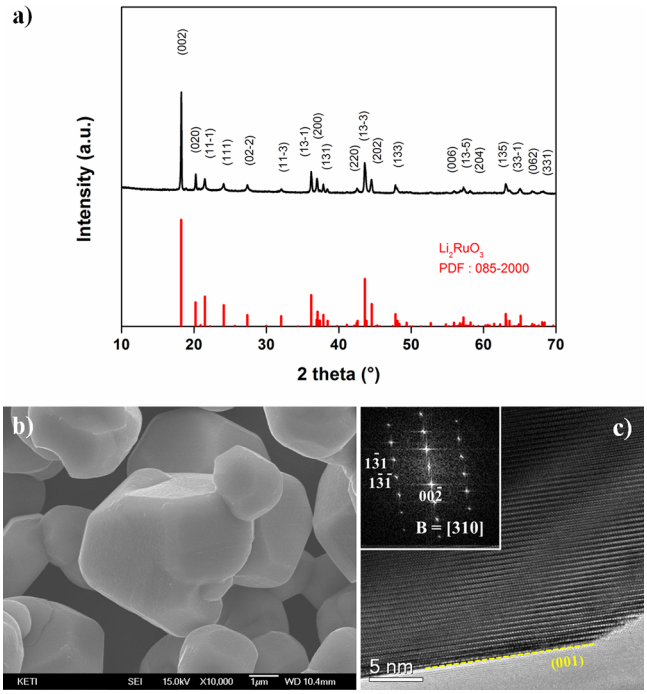

Figure 1. (a) Powder X-ray diffraction patterns of Li_2RuO_3, which has monoclinic symmetry (space group: *C*2/*c*). The red spectrum shows the line positions of the standard (JCPDS 85-2000). The morphology and microstructure of Li_2RuO_3: (b) FESEM image and (c) HRTEM image, together with the corresponding selected area diffraction pattern (SADP) in the inset.

performed using FESEM and HRTEM. The FESEM image displays rectangular Li_2RuO_3 particles with a particle size of a few micrometers and a smooth surface (Figure 1b) (S1 in the Supporting Information). The HRTEM image in Figure 1c, combined with the corresponding selected-area electron diffraction (SAED) patterns in the inset, reveals the fine microstructure and the strong crystallinity. Each particle is a monocrystal with monoclinic symmetry. Interestingly, the Li_2RuO_3 powder was faceted. From the viewpoint of total free energy, the tendency to minimize surface energy is the defining factor affecting the morphology. Herein, the (001) forms the facet to minimize the total surface energy in the Li_2RuO_3 powder. The periodic lattice image of Li_2RuO_3 shows the general characteristics of the layered structure. No evidence of extended defects was observed within the individual particle. From the results, we confirmed that single-phase Li_2RuO_3 with layered structure had been successfully synthesized under the optimized conditions.

Our major concern relating to Li_2RuO_3 as an additive for improving the energy density of LICs is to verify its high reversibility in electrochemical Li^+ insertion and extraction and its structural stability in the operating voltage window of the LIC. In our system, the cell should be charged to 4.7 V (vs Li/Li^+) for prelithiation of the NE prior to use. Li_2RuO_3 will inevitably be exposed to a high-voltage environment. By charging to 4.1 V, ~1.1 mol of Li^+ has been extracted from Li_2RuO_3.[23,24] Further Li^+ extraction, however, has not been investigated in voltage regions above 4.1 V. It is necessary, therefore, to investigate the electrochemical and structural properties of Li_2RuO_3 at the high voltage of 4.7 V. Figure 2a shows the galvanostatic charge and discharge profiles of Li_2RuO_3 collected at the first cycle (solid line) at a constant

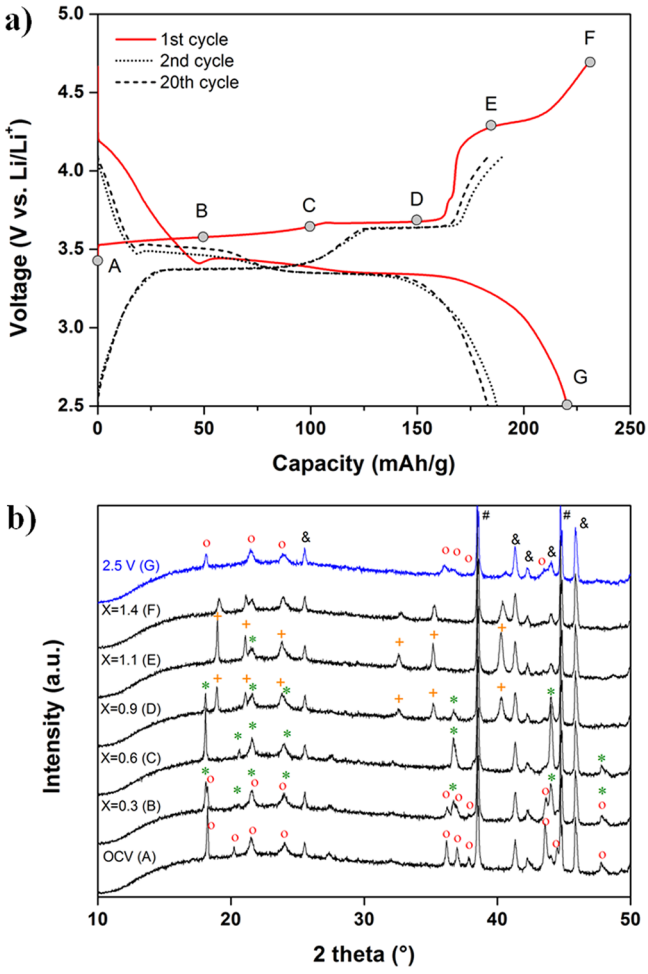

Figure 2. (a) Galvanostatic charge and discharge profiles for Li_2RuO_3 in the voltage range of 2.5−4.7 V for the first cycle (solid line) and in the voltage range of 2.5−4.1 V for the second (dotted line) and twentieth cycles (dashed line). (b) In situ XRD patterns collected at different SOCs ($Li_{2-x}RuO_3$, x = 0, 0.3, 0.6, 0.9, 1.1, 1.4) during the first charge and discharge, marked with Li_2RuO_3 (o), $Li_{1.4}RuO_3$ (*), and $Li_{0.9}RuO_3$(+) references.

current of 12.5 mA/g (0.05 C). The delivered charge capacity was estimated to be 231.0 mAh/g; this means that ~1.4 mol of Li could be extracted from Li_2RuO_3 during the first charge to 4.7 V, and 95.4% of Li^+ was reversibly recovered during the subsequent discharge to 2.5 V. From the second cycle (dotted line), it was cycled repeatedly in the voltage range of 2.5 to 4.1 V, and we observed only 2.0% of capacity fading after 20 cycles (dashed line). This observation reveals that Li_2RuO_3 is highly reversible for Li^+ insertion and extraction reaction in the given operating voltage. One may argue that the current electrolytes could be possibly unstable around 4.7 V (vs Li/Li^+). We carefully investigated the possible contribution of the electrolyte decomposition on the charge capacity of Li_2RuO_3. We found that the additional capacity due to the electrolyte decomposition is not significant (S2 in the Supporting Information).

We observed two distinctive plateaus at 3.5 and 3.6 V due to the multiphasic reaction between Li_2RuO_3 and $Li_{0.9}RuO_3$ upon Li^+ extraction up to 4.1 V, which is similar to previous reports. Interestingly, on further charging to 4.7 V, a new plateau clearly appeared at 4.3 V. To identify changes in the phase and composition of $Li_{2-x}RuO_3$ upon Li^+ extraction up to 4.7 V, we

dx.doi.org/10.1021/jp4005828 | J. Phys. Chem. C 2013, 117, 11471−11478

Table 1. Comparison of Lattice Parameters and Unit Cell Volumes Calculated from the XRD Patterns of $Li_{2-x}RuO_3$ (x = 1.1, 1.4)

$Li_{2-x}RuO_3$	lattice parameter a [Å]	lattice parameter b [Å]	lattice parameter c [Å]	unit cell volume [Å^3]
X = 1.1[a]	5.1016	5.1016	14.0301	316.23
X = 1.1	5.1001(3)	5.1001(3)	14.0280(3)	316.00
X = 1.4	5.0802(5)	5.0802(5)	13.9592(5)	312.01

[a]Reference: $Li_{0.9}RuO_3$ (JCPDS#85-2002)

performed in situ XRD on the Li_2RuO_3 electrodes prepared at a different state of charge (SOC) during the first charge, as presented in Figure 2b. According to the XRD pattern collected at the OCV (point A, x = 0), all reflections are indexed to only Li_2RuO_3 (JCPDS 85-2000). There is no visible evidence of the formation of any impurity or secondary phase. As the charge progressed to point B (x = 0.3), additional peaks, corresponding to $Li_{1.4}RuO_3$ with a monoclinic symmetry (JCPDS 85-2001), as a result of partial Li^+ extraction from Li_2RuO_3 were detected. After further Li^+ extraction (point C, x = 0.6), we observed the $Li_{1.4}RuO_3$ phase with a small amount of $Li_{0.9}RuO_3$, which has a rhombohedral symmetry (JCPDS 85-2002), but we did not detect the Li_2RuO_3 phase. These results indicated that there was a two-phase reaction between Li_2RuO_3 and $Li_{1.4}RuO_3$ when the cell was charged to point C (x = 0.6). From point D (x = 0.9), we found a phase transition from $Li_{1.4}RuO_3$ (monoclinic) to $Li_{0.9}RuO_3$ (rhombohedral), corresponding to a two-phase reaction between $Li_{1.4}RuO_3$ and $Li_{0.9}RuO_3$. When Li_2RuO_3 was further charged to points E (x = 1.1) and F (x = 1.4), no additional phase transformation or phase formation was found to take place based on the obtained reflections. Beyond point D (x = 0.9), the intensity of the (003), (110), and (11−3) peaks of $Li_{0.9}RuO_3$ gradually decreased, while its rhombohedral symmetry remained. A small reduction in lattice parameters and cell volume corresponding to Li^+ extraction from $Li_{0.9}RuO_3$ was observed, as summarized in Table 1. Note that the plateau observed at 4.3 V is associated with Li^+ extraction from $Li_{0.9}RuO_3$, and it is reversible without significant structural change. Even after 1.5 mol of Li^+ was extracted no further structural change occurred (S3 in the Supporting Information). After a subsequent discharge to 2.5 V (point G), we confirmed that all reflections were well-matched with the Li_2RuO_3 phase and other peaks associated with its delithiated phases, such as $Li_{1.4}RuO_3$ and $Li_{0.9}RuO_3$, disappeared. These results reveal that most of the Li^+ extracted from Li_2RuO_3 reversibly returned to their positions in the Li_2RuO_3 structure (S4 in Supporting Information). Thus, Li_2RuO_3 can be used as a promising additive for PE to provide additional faradaic reaction of Li^+ in the operating voltage window of the LIC.

The change in the chemical states of Ru metal in $Li_{2-x}RuO_3$ was also investigated using ex situ XPS during the first charge. The Ru 3d5/2 spectra collected from various SOC states were carefully fitted with the C1s spectra at 284.0 eV, as presented in Figure 3a. At OCV (point A), the binding energy of the Ru 3d5/2 component corresponds to 280.9 eV. This can be assigned to Ru^{4+}, which corresponds to the Li_2RuO_3 phase.[25] After partial Li^+ extraction (point B, x = 0.3), we confirmed the presence of a small amount of Ru with a higher oxidation state (Ru^{6+}), which led to an apparent shift in the binding energy to 282.1 eV. Upon further charging, the peak gradually shifted to higher binding energy because of the increase in the number of Ru^{6+}. After removal of 1.4 mol of Li^+ from Li_2RuO_3 by charging to 4.7 V (point F, x = 1.4), Ru mainly existed in the form of

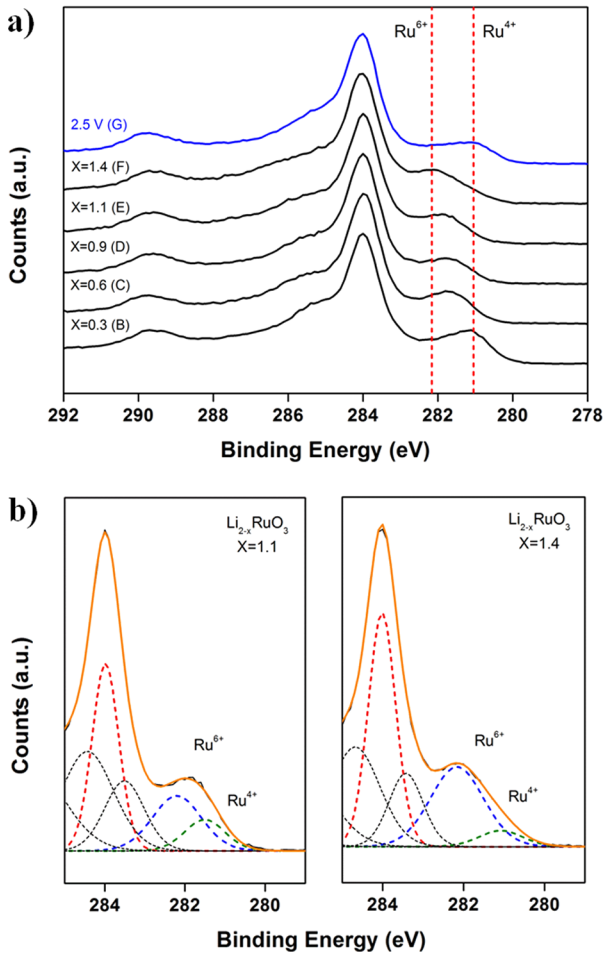

Figure 3. (a) Ex situ XPS spectra for the Ru 3d5/2 component collected at different SOCs ($Li_{2-x}RuO_3$, x = 0.3, 0.7, 1.0, 1.2) during the first charge and discharge and (b) comparison of the Ru 3d5/2 spectra collected from $Li_{2-x}RuO_3$ (x = 1.1 and 1.4).

Ru^{6+}, together with a relatively small amount of Ru^{4+}. Importantly, Ru^{6+} was reversibly reduced to Ru^{4+} after the subsequent discharge to 2.5 V (point G); this also supports the highly reversible reactions of Li_2RuO_3 for Li^+ insertion. These findings are consistent with the phase transitions of Li_2RuO_3 that accompany Li^+ extraction and insertion, as confirmed in the in situ XRD results above. In particular, we provide a comparison of Ru 3d5/2 spectra collected at points E (x = 1.1) and F (x = 1.4) after careful deconvolution in Figure 3b. It is clear that the peak intensity at 282.1 eV corresponding to the Ru^{6+} component increases along with further Li^+ extraction, in contrast with the notable reduction in the intensity of the Ru^{4+} peak. These results indicate that further Li^+ extraction from $Li_{0.9}RuO_3$ is also associated with the redox reactions between Ru^{4+} and Ru^{6+}.

dx.doi.org/10.1021/jp4005828 | J. Phys. Chem. C 2013, 117, 11471−11478

Table 2. Summary of Electrochemical Properties, Charge and Discharge Capacities, Irreversible Capacities, and Initial Coulombic Efficiency (ICE) of Li_2MoO_3 and Li_2RuO_3 at the First Cycle (0.1 C, 2.5 to 4.7 V vs. Li/Li^+)

	charge capacity [mAh/g]	discharge capacity [mAh/g]	irreversible capacity [mAh/g]	ICE [%][a]
Li_2MoO_3	267.1	85.0	182.1	31.8
Li_2RuO_3	231.0	220.3	10.7	95.4

[a]Initial coulombic efficiency = discharge capacity/charge capacity.

For practical use of the Li_2RuO_3 additive, we conducted fundamental studies on the electrochemical properties of Li_2RuO_3. (The results are summarized in Table 2.) In relation to the electrochemical properties of Li_2MoO_3 and Li_2RuO_3, it should be noted that Li_2MoO_3 exhibits a large initial charge capacity of 267.1 mAh/g, with a large irreversible capacity of 182.1 mAh/g in the voltage range of 2.5 to 4.7 V (vs Li/Li^+). This is essential for its use as a Li^+ provider. Most of the Li^+ electrochemically extracted from Li_2MoO_3 during the first charging would be used for prelithiation of the NE.[6] In contrast, Li_2RuO_3 is highly reversible in terms of Li^+ insertion and extraction in the same voltage region. Approximately 231.0 mAh/g of initial charge capacity was obtained with an initial Coulombic efficiency (ICE) of 95.4% (S5 in the Supporting Information). In addition, Li_2RuO_3 also shows low-capacity fading even at high current density during cycling. We expect that additional faradaic reaction can be independently promoted by incorporation of Li_2RuO_3 into the PE during cycling. Although it is not a typical capacitive reaction, the redox reaction of Ru^{4+}/Ru^{6+} allows reversible Li^+ insertion and extraction in the PE, as reflected in the improvement of the deliverable capacitance. Therefore, we believe that Li_2RuO_3 is a favorable additive for improving the energy density of the LIC.

We designed and prepared PEs with different amounts of Li_2RuO_3 (0, 5, and 10 wt %) to examine the effects of the Li_2RuO_3 additive on the electrochemical performance of the LIC. For comparative purposes, the same amounts of activated carbon and Li_2MoO_3 were incorporated into the PEs (Table S1 in the Supporting Information). CVs obtained at the first cycle are compared in Figure 4a. To ensure Li^+ predoping of the NE, the cells were initially oxidized to 4.7 V (vs Li/Li^+) and then reduced to 2.5 V at a scan rate of 0.05 mV/s, corresponding to 0.1 C. According to the CV profiles, the cell without Li_2RuO_3 (Figure 4a, black solid line) shows a notable oxidation peak at ~4.2 V, which is attributable to Li^+ extraction from Li_2MoO_3. The corresponding reduction peak, however, was not observed upon subsequent discharging. This result is directly related to the irreversible nature of Li_2MoO_3. The cells with Li_2RuO_3 additive have an additional pair of oxidation and reduction peaks at ~3.7 V. These peaks can be attributed to the redox reaction of Ru^{4+}/Ru^{6+} in Li_2RuO_3, and they reveal that Li_2RuO_3 promotes an additional faradaic reaction through Li^+ insertion and extraction. Figure 4b,c presents a comparison of the CV profiles of the cells measured at scan rates of 0.09 (0.2 C) and 4.4 mV/s (10 C), respectively. The CV profiles have rectangular shapes, which are desirable for capacitor applications.[26,27] As seen in Figure 3b, the achieved capacitance increases in proportion to the amount of Li_2RuO_3 in the PE. The higher specific capacitance of 381.2 F/g compared with that of the LIC without the additive (328.6 F/g) can be attained by incorporation of 10 wt % Li_2RuO_3. It is reasonable to infer that the additional capacitance of ~52.6 F/g mainly originates from the reversible faradaic reactions involved in Li_2RuO_3. Pseudocapacitance induced by absorption and desorption of anions on $Li_{2-x}RuO_3$ also partially contributes to the increased capacitance. The CV profiles still have quasi-rectangular shapes even at the high scan rate of 4.4 mV/s (10 C), and the additional capacitance associated with incorporation of Li_2RuO_3 additive is still obvious (Figure 4c). Our observations support the view that fast charging and discharging of the LIC could be allowed without a significant equivalent series resistance of the PE after incorporation of Li_2RuO_3, making it favorable for use as an additive in the LIC, which needs high power capability.

Another important issue to be considered is determination of the effects of Li_2RuO_3 addition on the electrochemical impedance of the LIC during operation. This is because it significantly affects some aspects of cell performance such as rate capability and cyclic performance. Useful information that helps us to understand the role of Li_2RuO_3 in improving electrochemical performance of LIC can be acquired from the ac-impedance analysis of the PEs. Figure 5a presents the Nyquist plots of the ac-impedance spectra obtained from the PEs containing different amounts of Li_2RuO_3 additive after the first charge to 4.7 V for Li^+ predoping. Each of the ac-impedance spectra consists of two separated arcs in the high-frequency range and a straight line inclined at a constant angle to the real axis in the low-frequency range. In general, the first arc is mainly attributed to the passive film on the surface of the oxide particle and the second arc is ascribed to the interfacial charge-transfer reaction combined with double-layer charging/discharging. A straight line at low frequencies is associated with semi-infinite diffusion of lithium in the electrode (Warburg impedance). The Li_2RuO_3 additive strongly affects the interfacial charge-transfer reaction (rather than the passive film formation), as evidenced by a reduced size of the second arc with increasing amount of Li_2RuO_3. The impedance spectra were quantitatively analyzed using the equivalent circuit in the inset. In the equivalent circuit, R_1 represents the uncompensated solution resistance; R_2 and CPE_1 are the resistance and the constant phase element for surface films, respectively; R_3 and CPE_2 are the charge-transfer resistance and the constant phase element for double-layer charging/discharging, respectively; and ZFD represents the diffusion impedance. The R_3 values estimated by complex nonlinear least-squares (CNLS) fitting of the ac-impedance spectra are shown in Figure 5b. We found that the value of R_3 measured after charging to 4.7 V was significantly reduced by Li_2RuO_3 addition. It appears that strong Ru−Ru metallic boding in the delithiated form of $Li_{2-x}RuO_3$ (x = 1.4) could effectively facilitate charge-transfer kinetics in the PE. In addition, the result indicates that conductivity loss due to the Li_2RuO_3 additive is not significant. When subsequently discharged to 2.5 V, the Li_2RuO_3-incorporated PEs exhibited lower R_3 values than the Li_2RuO_3-free PE did. Even after charging again to 4.1 V the variation of R_3 was negligible. These results indicate that the Li_2RuO_3 additive fulfills two important characteristics. These results also confirm that Li_2RuO_3 is an appropriate additive that shows two important features: (i) it provides highly reversible

dx.doi.org/10.1021/jp4005828 | J. Phys. Chem. C 2013, 117, 11471−11478

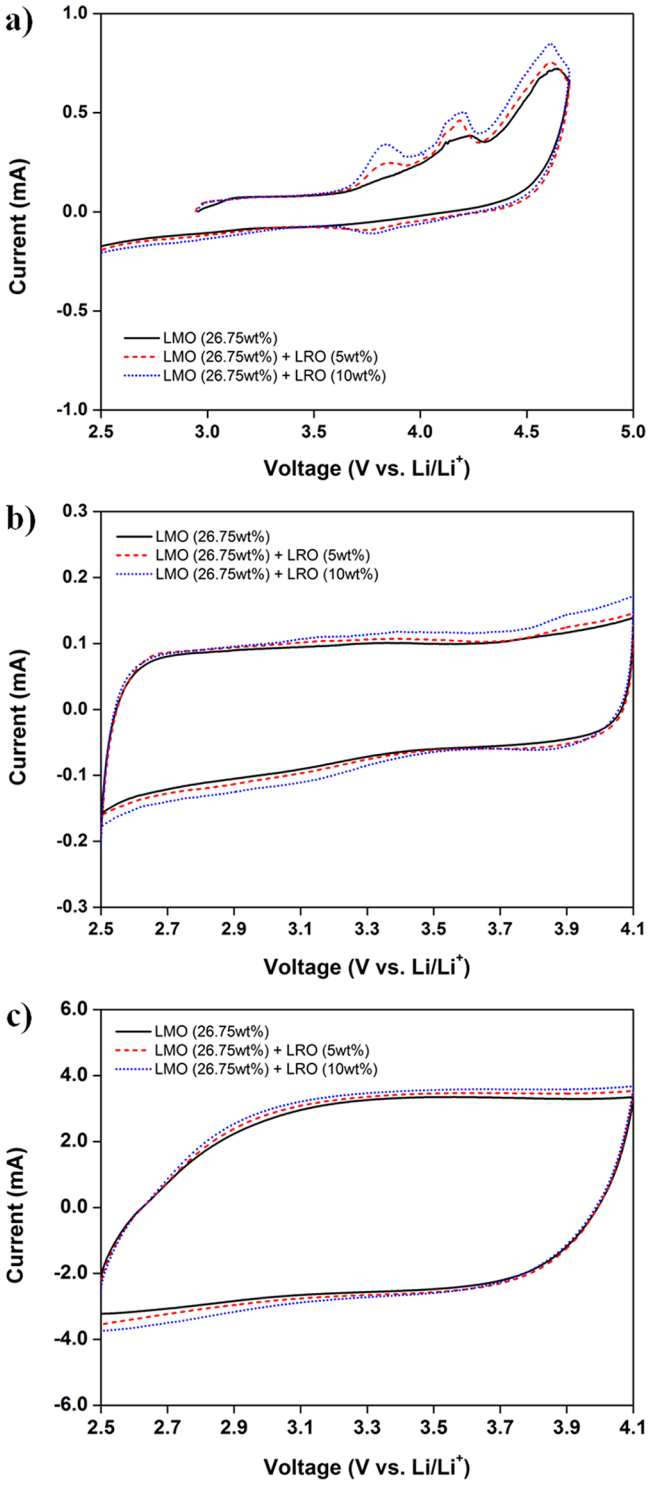

Figure 4. Cyclic voltammograms (CVs) for LIC half cells employing different amounts of Li_2RuO_3: 0, 5, and 10 wt % after Li^+ doping with Li_2MoO_3 (26.75 wt %) in the voltage range of 2.5−4.1 V. (a) CV profiles recorded with a scan rate of 0.05 mV/s at the first cycle. (b) CV profiles recorded with a scan rate of 0.09 mV/s and (c) CV profiles recorded with a scan rate of 4.4 mV/s.

Li^+ insertion and extraction; and (ii) it secures a conductive environment in the operating voltage range of the LIC.

Figure 6a shows the galvanostatic charge and discharge profiles of the LIC full cells having PEs with Li_2MoO_3 (Li^+ source) and Li_2RuO_3 (additive). The amount of Li_2MoO_3 was

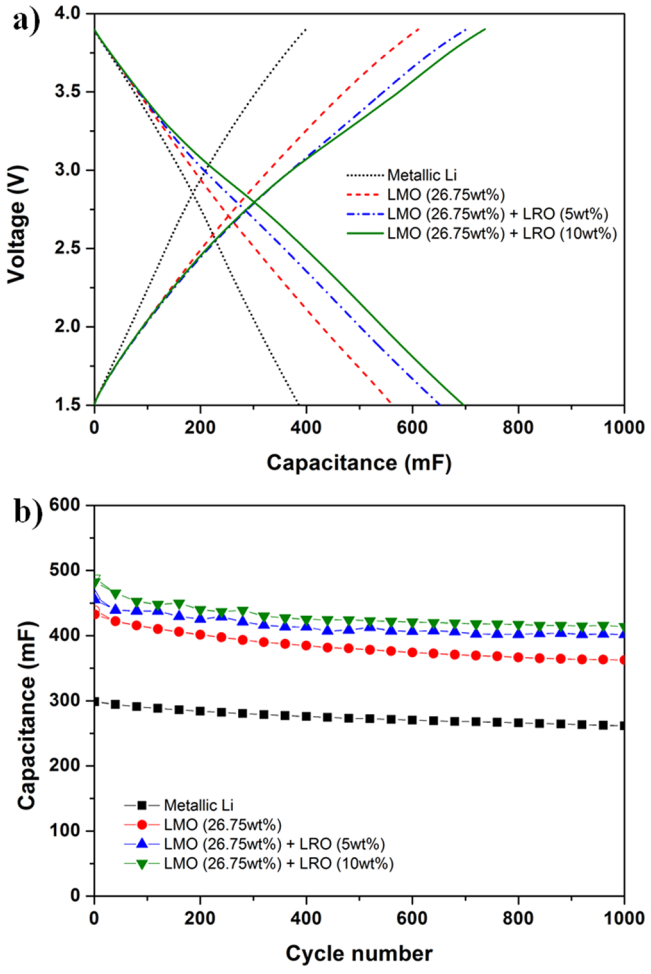

Figure 5. Electrochemical impedance spectra for LIC half cells employing different amounts of Li_2RuO_3, 0, 5, 10 wt %: (a) Nyquist plots collected after charging to 4.7 V versus Li/Li^+, which are carefully fitted with an equivalent circuit (inset). (b) Comparison of charge-transfer resistance (R_3) at different states.

fixed at 25.6 wt % and the amounts of Li_2RuO_3 was varied to demonstrate the effects of Li_2RuO_3 addition on the cell performance. For proper operation, the cells were initially charged up to 4.7 V (vs Li/Li^+) at a constant current density of 5.3 mA/g (0.1 C) and, then discharged to 2.5 V (vs Li/Li^+). The cells containing Li_2RuO_3 additive exhibited higher charge and discharge capacitances than those of the cell without Li_2RuO_3. It should be noted that the achieved capacitances of the cells proportionally increased as the content of Li_2RuO_3 increased. After the addition of Li_2RuO_3, we also observed an inflection point in the charge and discharge profiles at ~3.5 V, which could be attributed to the redox reaction of Ru^{4+}/Ru^{6+} in the PEs containing Li_2RuO_3 as an additive. The change in slope becomes larger on increasing the Li_2RuO_3 content. This reveals that Li_2RuO_3 reversibly contributes to additional capacitance in the operating voltage window of the LIC (1.5 to 3.9 V). Moreover, the redox reaction of Li_2RuO_3 is essential for increasing the deliverable capacitance of the PE, leading to the improvement of the electrochemical energy (S6 in the Supporting Information). Figure 6b shows the cycling performance of LIC full cells employing PEs with various amounts of Li_2RuO_3 additive. The cells were cycled at a constant current density of 530 mA/g (10 C) in the voltage range between 1.5 and 3.9 V. The delivered capacitance was clearly enhanced by

dx.doi.org/10.1021/jp4005828 | J. Phys. Chem. C 2013, 117, 11471−11478

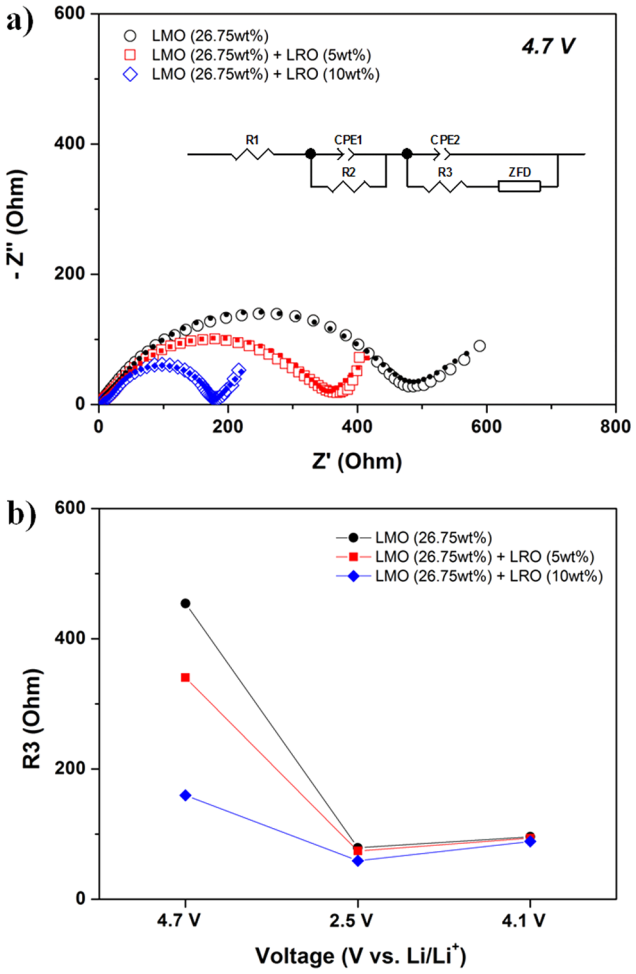

Figure 6. Electrochemical performance of LIC full cells employing different amounts of Li_2RuO_3, 0 wt % (●), 5 wt % (▲), and 10 wt % (▼), after Li^+ predoping with Li_2MoO_3 (26.75 wt %) in the voltage range of 1.5−3.9 V: (a) galvanostatic charge and discharge profiles with a constant current of 0.1 C (1 C = 53 mA/g), (b) cycling performance at a current density of 10 C over 1000 cycles. An LIC conventionally doped with metallic lithium is included as a reference (■) (open symbols: charge capacity, solid symbols: discharge capacity).

the addition of Li_2RuO_3, and the cells showed excellent cycling performance over 1000 cycles with relatively stable cyclic efficiency. Meanwhile, gradual increases in the anodic and cathodic voltages of the cell were observed during cycling; these indicate that the amount of Li^+ involved in the anodic reaction was continuously reduced (S7 in the Supporting Information).

Ragone plots for the LICs with advanced PEs designed with Li_2MoO_3 and Li_2RuO_3 are presented in Figure 7. The data were plotted as a function of achieved capacitances at different current densities, namely, 0.2, 0.5, 1.0, 5.0, 10, 20, and 40 C. First, the volumetric energy density of LICs can be significantly improved by elimination of metallic lithium from the cell. Li^+ predoping with Li_2MoO_3 exhibits efficient doping characteristics and better power density compared with the conventional method using metallic lithium. Second, the addition of Li_2RuO_3 is effective for increasing the capacitance of the LIC without sacrificing of the power characteristics. The metallic feature of $Li_{2-x}RuO_3$ may be responsible for the power enhancement in the partially lithiated state of the PEs. Surprisingly, the composite PEs could exhibit more than four times the

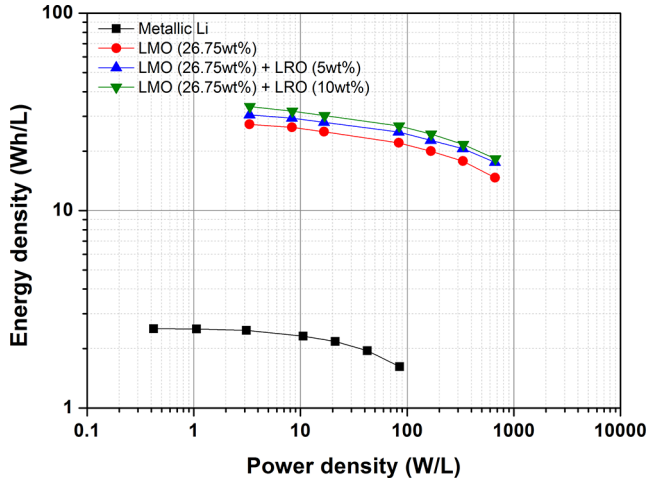

Figure 7. Ragone plots for the LIC full cells (with data plotted as a function of the achieved capacitances at different current densities of 0.2, 0.5, 1.0, 5.0, 10, 20, and 40 C). A LIC conventionally doped with metallic lithium is includes as a reference (■).

volumetric energy density compared with those of conventional LICs at the same power level. We expect that further improvements in the cell performance could be achieved after the optimization of particle size for both transition metal oxides.

■ CONCLUSIONS

In summary, the high reversibility of Li_2RuO_3 for Li^+ insertion and extraction for use as an additive in advanced LICs is confirmed in the voltage range of 2.5−4.7 V (vs Li/Li^+). We observed a new plateau associated with further Li^+ extraction from $Li_{0.9}RuO_3$ above 4.3 V (vs Li/Li^+). No significant structural change occurs even after 1.4 mol of Li^+ is extracted from Li_2RuO_3, and most of the extracted Li^+ is recovered during subsequent discharging. These characteristics allow further improvement in the energy density of the LICs by promoting additional faradaic reactions of Li^+ in the PE. In addition, the metallic feature of $Li_{2-x}RuO_3$ is may be responsible for effectively facilitating charge-transfer kinetics in the PE, leading to power enhancement. Accordingly, we believe that Li_2RuO_3 is a suitable additive for maximizing the electrochemical performance of LICs.

■ ASSOCIATED CONTENT

Ⓢ Supporting Information

Additional FESEM images, particle size distributions, electrochemical behaviors of Li_2MoO_3 and Li_2RuO_3, and table of electrode compositions. This material is available free of charge via the Internet at http://pubs.acs.org.

■ AUTHOR INFORMATION

Corresponding Author

*E-mail: js_energy@keti.re.kr (J.-S.K.), yjkim@keti.re.kr (Y.-J.K.). Tel: +82 31 789 7491. Fax: +82 31 789 7499.

Notes

The authors declare no competing financial interest.

■ ACKNOWLEDGMENTS

This research was supported by the Converging Research Center Program through the Ministry of Education, Science and Technology (2012K001264), Republic of Korea.

REFERENCES

(1) Winter, M.; Brodd, R. What Are Batteries, Fuel Cells, and Supercapacitors? *J. Chem. Rev.* **2004**, *104*, 4245−4269.

(2) Amatucci, G. G.; Badway, F.; Pasquier, A. D.; Zheng, T. An Asymmetric Hybrid Nonaqueous Energy Storage Cell. *J. Electrochem. Soc.* **2001**, *148*, A930−A939.

(3) Burke, A. R&D Considerations for the Performance and Application of Electrochemical Capacitors. *Electrochim. Acta* **2007**, *53*, 1083−1091.

(4) Simon, P.; Gogosti, Y. Materials for Electrochemical Capacitors. *Nat. Mater.* **2008**, *7*, 845−854.

(5) Aida, T.; Murayama, I.; Yamada, K.; Morita, M. Analyses of Capacity Loss and Improvement of Cycle Performance for a High-voltage Hybrid Electrochemical Capacitor. *J. Electrochem. Soc.* **2007**, *154*, A798−A804.

(6) Park, M. S.; Lim, Y. G.; Kim, J. H.; Kim, Y. J.; Cho, J.; Kim, J. S. A Novel Lithium-Doping Approach for an Advanced Lithium Ion Capacitor. *Adv. Energy Mater.* **2011**, *1*, 1002−1006.

(7) James, A. C. W. P.; Goodenough, J. B. Structure and Bonding in Li_2MoO_3 and $Li_{2-x}MoO_3$ ($0 \leq x \leq 1.7$). *J. Solid State Chem.* **1988**, *76*, 87−96.

(8) Hibble, S. J.; Fawcett, I. D. Local Order and Metal-Metal Bonding in Li_2MoO_3, $Li_4Mo_3O_8$, $LiMoO_2$, and H_2MoO_3, Determined from EXAFS Studies. *Inorg. Chem.* **1995**, *34*, 500−508.

(9) Park, K. S.; Im, D.; Benayad, A.; Dylla, A.; Stevenson, K. J.; Goodenough, J. B. $LiFeO_2$-Incorporated Li_2MoO_3 as a Cathode Additive for Lithium-Ion Battery Safety. *Chem. Mater.* **2012**, *24*, 2673−2683.

(10) Kobayashi, H.; Tabuchi, M.; Shikano, M.; Nishimura, Y.; Kageyama, H.; Ishida, T.; Nakamura, H.; Kurioka, Y.; Kanno, R. Synthesis and Electrochemical Properties of Lithium Molybdenum Oxides. *J. Power Sources* **1999**, *81*−*82*, 524−529.

(11) Zheng, J. P.; Cygan, P. J.; Jow, T. R. Hydrous Ruthenium Oxide as an Electrode Material for Electrochemical Capacitors. *J. Electrochem. Soc.* **1995**, *142*, 2699−2703.

(12) Lee, H. Y.; Goodenough, J. B. Supercapacitor Behavior with KCl Electrolyte. *J. Solid State Chem.* **1999**, *144*, 220−223.

(13) Rudge, A.; Raistrick, I.; Gottesfeld, S.; Ferraris, J. P. A Study of the Electrochemical Properties of Conducting Polymer for Application in Electrochemical Capacitors. *Electrochim. Acta* **1994**, *39*, 273−287.

(14) Nishide, H.; Iwasa, S.; Pu, Y. J.; Suga, T.; Nakahara, K.; Satoh, M. Organic Radical Battery: Nitroxide Polymers as a Cathode-active Material. *Electrochim. Acta* **2004**, *50*, 827−831.

(15) Moore, G. J.; Johnson, C. S.; Thackeray, M. M. The Electrochemical Behavior of $x LiNiO_2 \cdot (1-x) Li_2RuO_3$ and $Li_2Ru_{1-y}Zr_yO_3$ Electrodes in Lithium Cells. *J. Power Sources* **2003**, *119*−*121*, 216−220.

(16) Stux, A. M.; Swider-Lyons, K. E. Improved High Power Li-ion Batteries with Li_2RuO_3 Addition: A Fast Charging and Fast Cycling Study. *J. Power Sources* **2007**, *165*, 635−639.

(17) Wang, G. X.; Zhang, B. L.; Yu, Z. L.; Qu, M. Z. Manganese Oxide/MWNTs Composite Electrodes for Supercapacitors. *Solid State Ionics* **2005**, *176*, 1169−1174.

(18) Stux, A. M.; Swider-Lyons, K. E. Li-ion Capacity Enhancement in Composite Blends of $LiCoO_2$ and Li_2RuO_3. *J. Electrochem. Soc.* **2005**, *152*, A2009−A2016.

(19) James, A. C. W. P.; Goodenough, J. B. Structure and Bonding in Lithium Ruthenate, Li_2RuO_3. *J. Solid State Chem.* **1988**, *74*, 287−294.

(20) Johannes, M. D.; Stux, A. M.; Swider-Lyons, K. E. Electronic Structure and Properties of Li-insertion Materials: Li_2RuO_3 and RuO_2. *Phys. Rev. B* **2008**, *77*, 075124.

(21) Boulineau, A.; Croguennec, L.; Delmas, D.; Weill, F. Reinvestigation of Li_2MnO_3 Structure: Electron Diffraction and High Resolution TEM. *Chem. Mater.* **2009**, *21*, 4216−4222.

(22) Shannon, R. D.; Prewitt, C. T. Effective Ionic Radii in Oxides and Fluorides. *Acta Crystallogr.* **1969**, *B25*, 925−946.

(23) Kobayashi, H.; Kanno, R.; Kawamoto, Y.; Tabuchi, M.; Nakamura, O.; Takano, M. Structure and Lithium Deintercalation of $Li_{2-x}RuO_3$. *Solid State Ionics* **1995**, *82*, 25−31.

(24) Kobayashi, H.; Kanno, R.; Kawamoto, Y.; Tabuchi, M.; Nakamura, O. Physical Properties of the De-lithiated $Li_{2-x}RuO_3$ with the Layered Structure. *Solid State Ionics* **1996**, *86*−*88*, 859−863.

(25) Arico, A. S.; Vaglio, V.; Blasi, A. D.; Modica, E.; Antonucci, P. L.; Antonucci, V. Analysis of the High-temperature Methanol Oxidation Behaviour at Carbon-Supported Pt−Ru Catalysts. *J. Electroanal. Chem.* **2003**, *557*, 167−176.

(26) Yu, D.; Dai, L. Self-Assembled Graphene/Carbon Nanotube Hybrid Films. *J. Phys. Chem. Lett.* **2010**, *1*, 467−470.

(27) Kim, Y. T.; Mitani, T. Competitive Effect of Carbon Nanotubes Oxidation on Aqueous EDLC Performance: Balancing Hydrophilicity and Conductivity. *J. Power Sources* **2006**, *158*, 1517−1522.